Lecture 3: Neutrinos and Gravitational Waves from Core-Collapse Supernovae

Bernhard Müller

Monash University

ICTS Summer School on Gravitational-Wave Astronomy 2022
Lectures on Core-Collapse Supernovae

Recommended Reviews

For more in-depth reading and extensive references, which we cannot provide here, consult the following reviews on gravitational waves from supernovae:

- Abdikamalov, Pagliaroli & Radice, "Gravitational Waves from Core-Collapse Supernovae ", in "Handbook of Gravitational Wave Astronomy" (Eds. Bambi, Katsanevas &vKokkotas; Springer Singapore, 2021).
- Kotake 2013, Comptes rendus Physique, Volume 14, Issue 4, p. 318-351.

For supernova neutrinos consult:

- Müller 2019, Annual Review of Nuclear and Particle Science, vol. 69, p.253-278.
- Mirizzi et al. 2016, La Rivista del Nuovo Cimento, Volume 39, Issue 1-2, pp.1-112.
- Scholberg 2012, Annual Review of Nuclear and Particle Science, vol. 62, p.81-103.

Rotational Bounce Signal

mass quadrupole moment (transverse-trace free component)

Asymmetry parameter

radius

typical frequency

$$h \sim \frac{2G}{c^4 r} \frac{d^2 I}{dt^2} \sim \frac{2G}{c^4 r} \epsilon M R^2 f^2$$

dimensionless strain

distance

mass involved

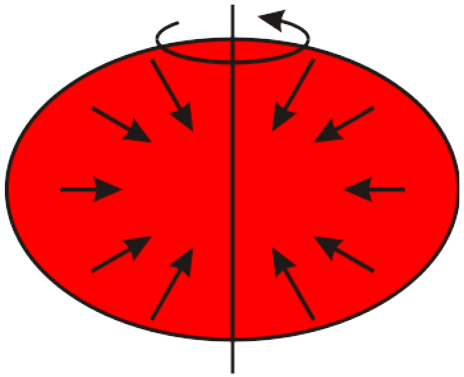

Rotational collapse

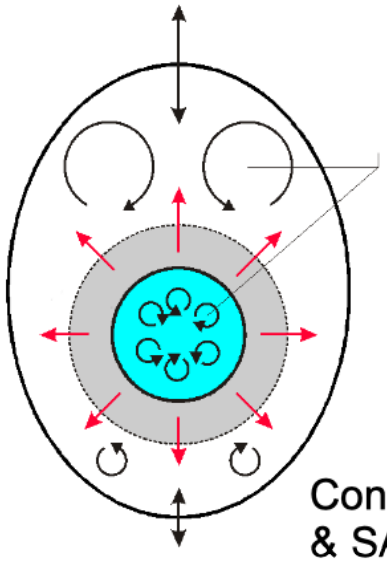

Convection & SASI

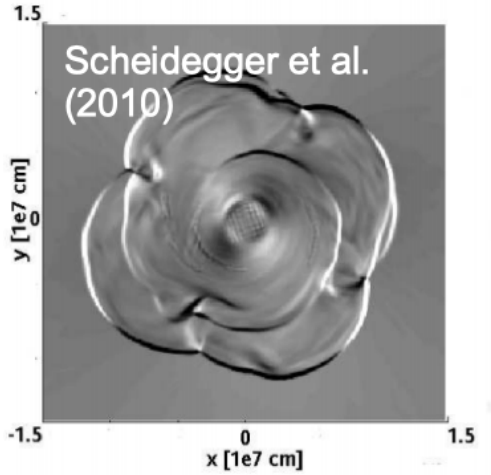

Other triaxial instabilities (low T/W, r-mode)

Rotational Bounce Signal

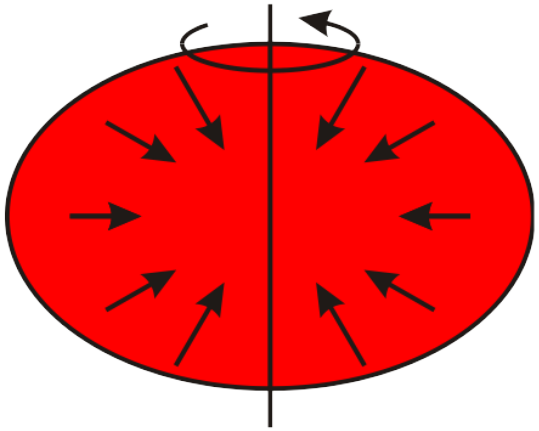

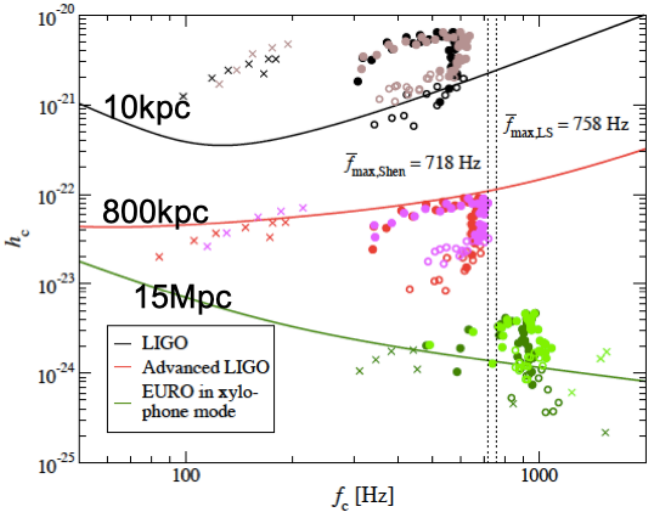

Characteristic strain & frequency for different progenitors, EoS & rotation rates (Dimmelmeier et al. 2008)

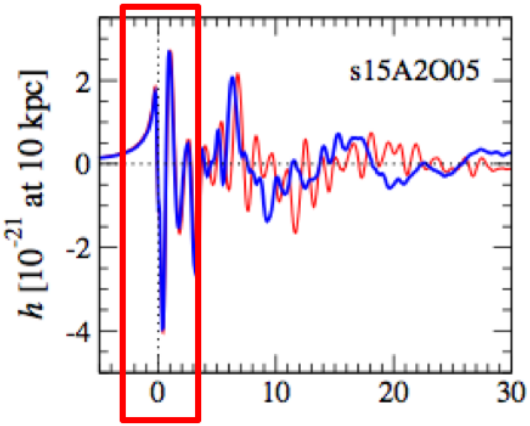

Bounce signal (Dimmelmeier et al. 2008): very regular shape, amenable to template-based searches

Detectability limit: of order ~40kpc for Advanced LIGO for initial core rotation periods of ~seconds (see, e.g., Logue et al. 2012, Hayama et al. 2015, Gossan et al. 2016)

At ~10kpc, the initial period can be constrained to within ~20% (Abdikamalov et al. 2014)

Rotational Bounce Signal

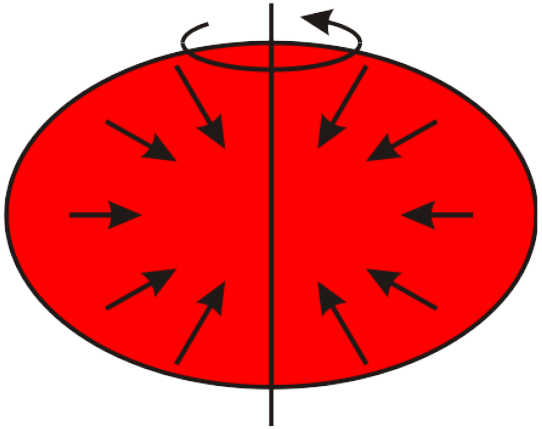

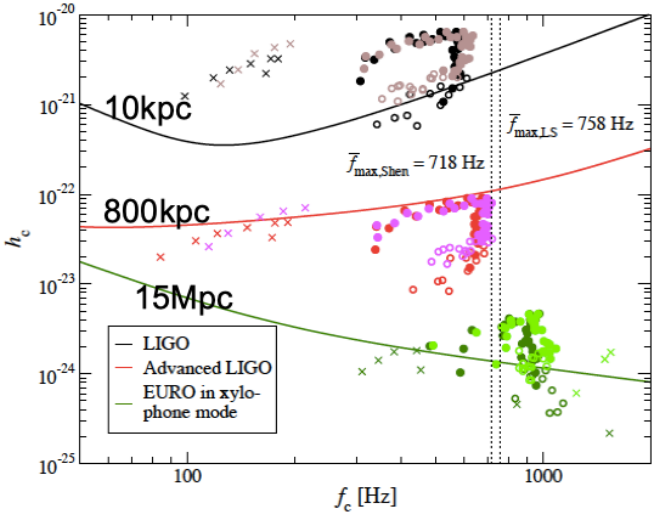

Characteristic strain & frequency for different progenitors, EoS & rotation rates (Dimmelmeier et al. 2008)

Can infer rotational state of progenitor!

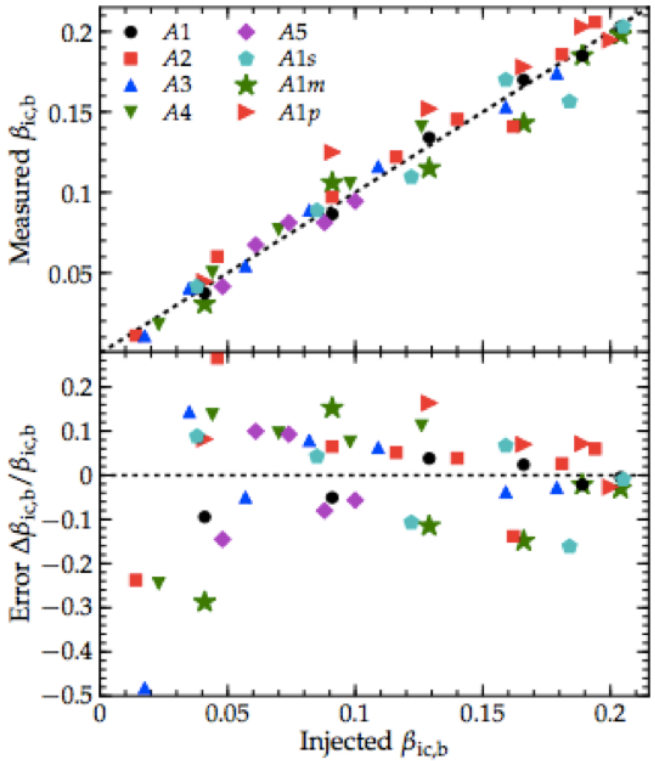

Abdikamlov et al. (2014): Inferred β=T/W in progenitor coe from prospective signal

GW Emission: Post-Bounce Phase

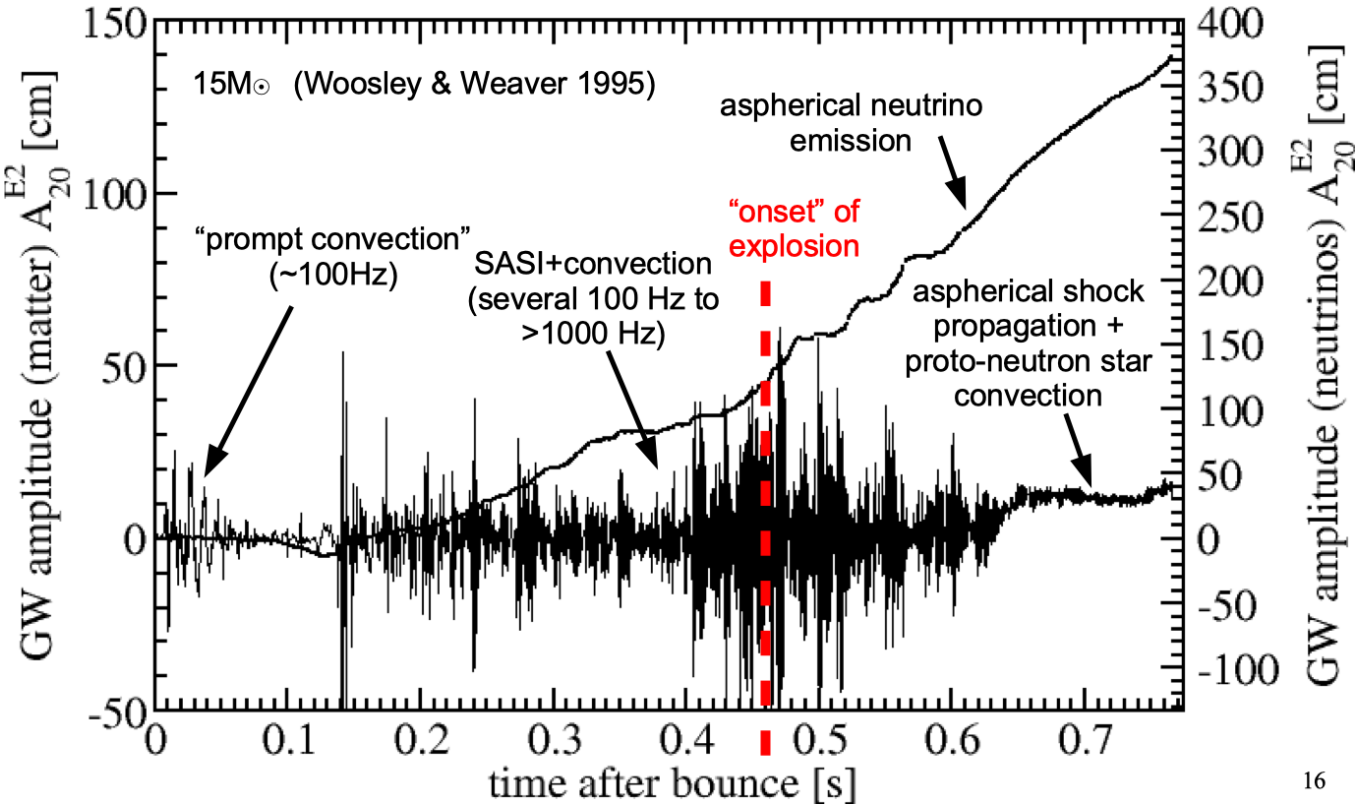

Amplitudes $A = h \times D$ for 2D model, ampitudes in 3D are lower, but structure is similar.

Understanding the Time-Frequency Structure of the Signal

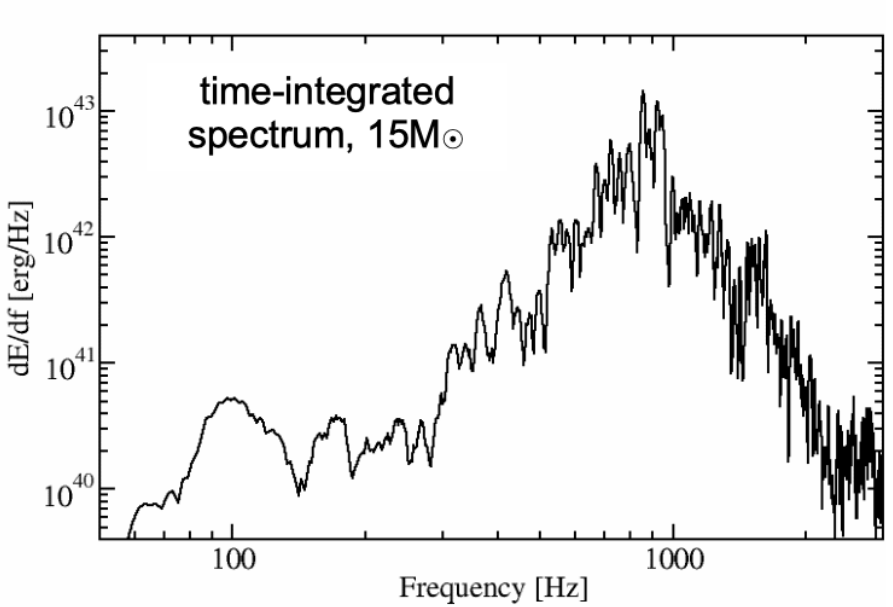

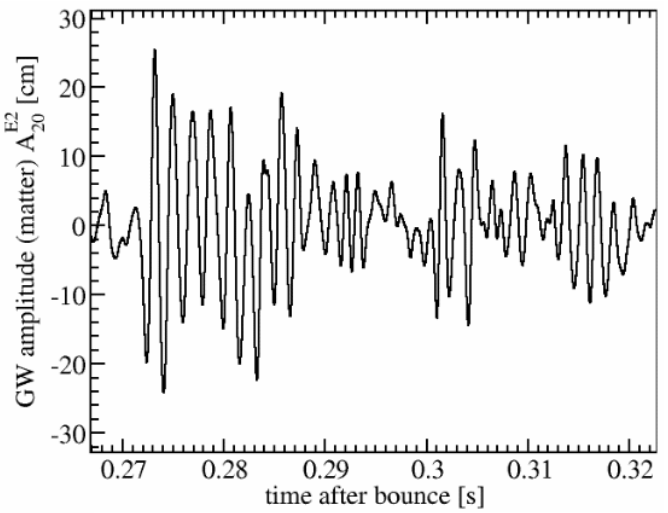

zooming in on an exemplary time interval...

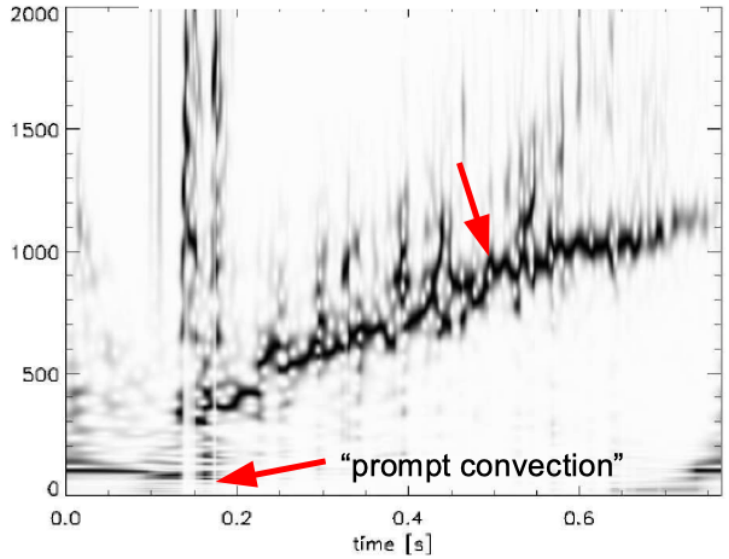

normalized wavelet spectrogram, 15M⊙

Signal seems to contain a lot of broad-band noise, but there is a well-defined and sharp frequency structure underneath:

- Better time-frequency analysis helps!
- Normalized wavelet spectrogram clearly shows evolution of typical frequency

Origin of Post-bounce GW Emission

- An early low-frequency signal at $\sim 100 \ldots 200\,\mathrm{Hz}$ is trigged by prompt convection behind the shock. The convection excites quadrupolar p-modes (acoustic modes) between the shock and proto-neutron star.
- The bulk of the signal is associated with the activity of convection and SASI. Emission tends to be strongest around the time of shock revival and subsides afterwards.
- The asymmetric emission of neutrinos and the asymmetric expansion of the shock during the explosion phase can generate a tail signal (memory effect).

Post-bounce phase: High-frequency Signal

The high-frequency signal comes quadrupole oscillations modes excited by convection and SASI. The dominant mode is typically the fundamental mode (f-mode) or a the ${}^2g_2$ gravity mode (Torres-Forne et al. 2018, Morozova et al. (2018). The mode frequency is related to the PNS parameters:

$$f \approx 2\pi \frac{GM}{R^2} \sqrt{1.1 \frac{m_n}{\langle E_{\bar{\nu}_e} \rangle}} \left(1 - \frac{GM}{Rc^2}\right),$$

where the electron antineutrino mean energy $\langle E_{\bar{\nu}_e} \rangle$ is a potentially measurable proxy for the PNS surface temperature (Mueller et al. 2013)

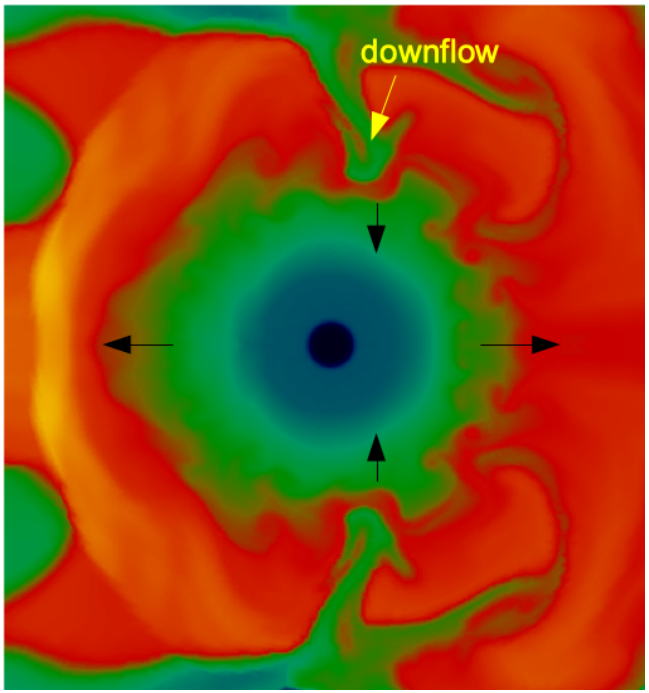

Emitted Graviational Wave Energy

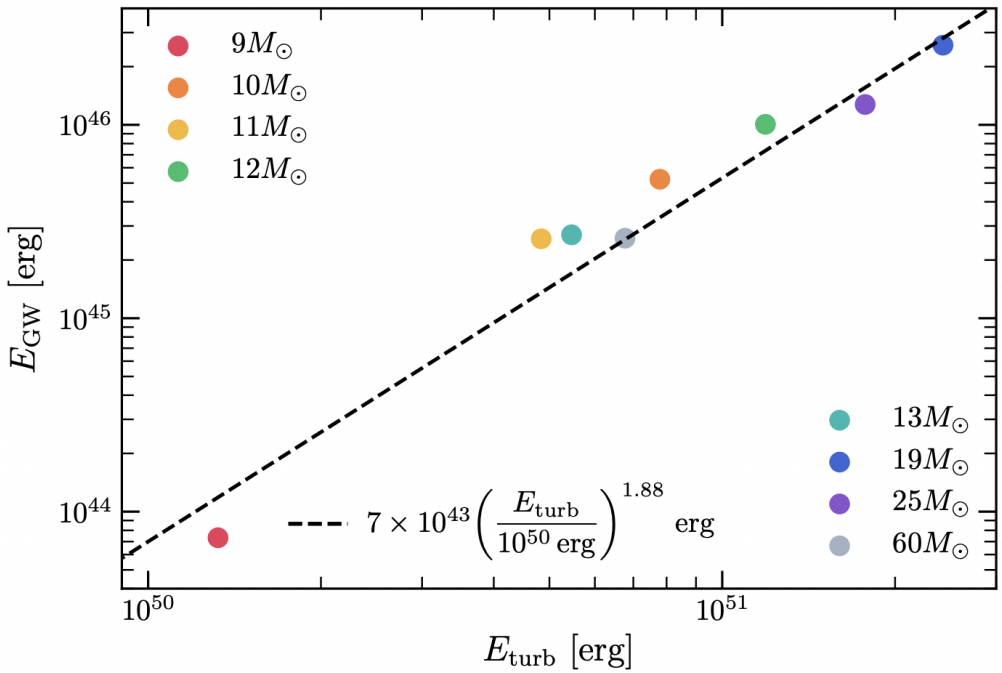

The emitted GW energy scales with the time-integrated turbulent kinetic energy flux onto the PNS (Radice et al. 2019):

$$E_{\rm GW} = 3 \times 10^{43}\,{\rm erg} \left(\frac{\int F_{\rm turb}\,{\rm d}t}{10^{50}\,{\rm erg}} \right)^{1.88}.$$

This can be derived from the theory of g-mode excitation by convection (Powell & Mueller 2019).

Progenitor dependence

Empirically, the post-bounce GW signal tends to be stronger for more massive progenitors, and stronger for exploding ones than for non-exploding ones.

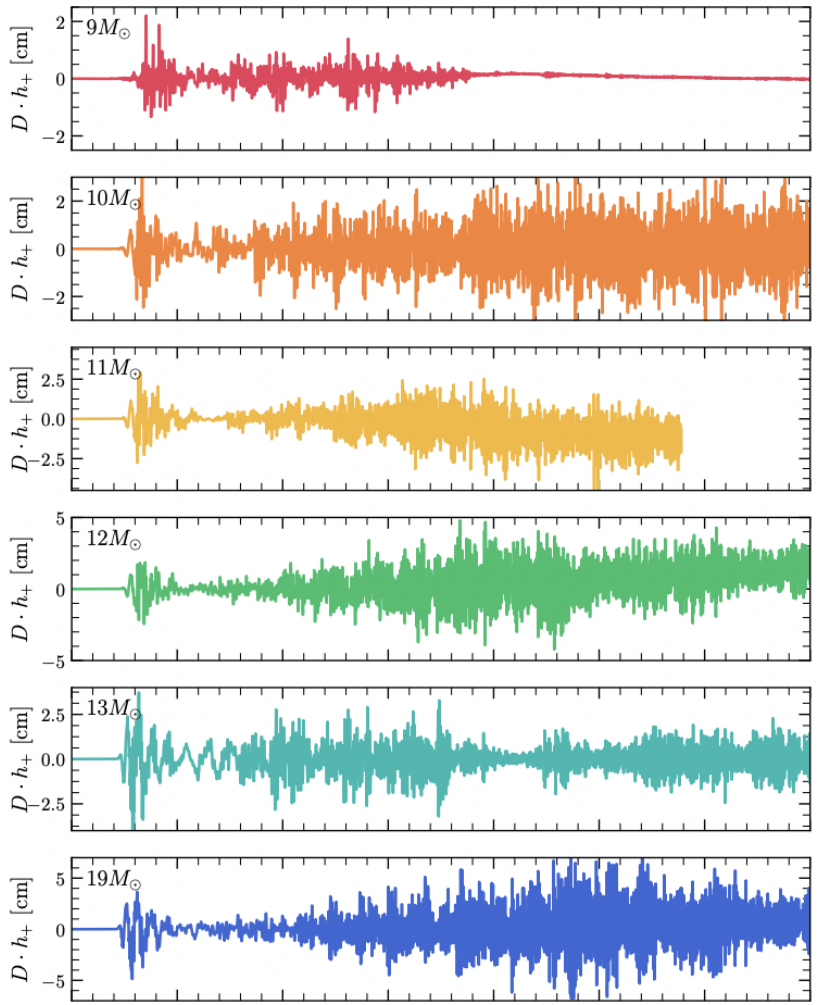

Credit: Radice et al. (2019)

SASI Signal

Models with a strong SASI show additional low-frequency emission, typically at $100 \ldots 200\,\mathrm{Hz}$ (Kuroda et al. 2016, Andresen et al. 2018). Because of frequency doubling, the GW frequency cannot always be identified directly with the SASI frequency.

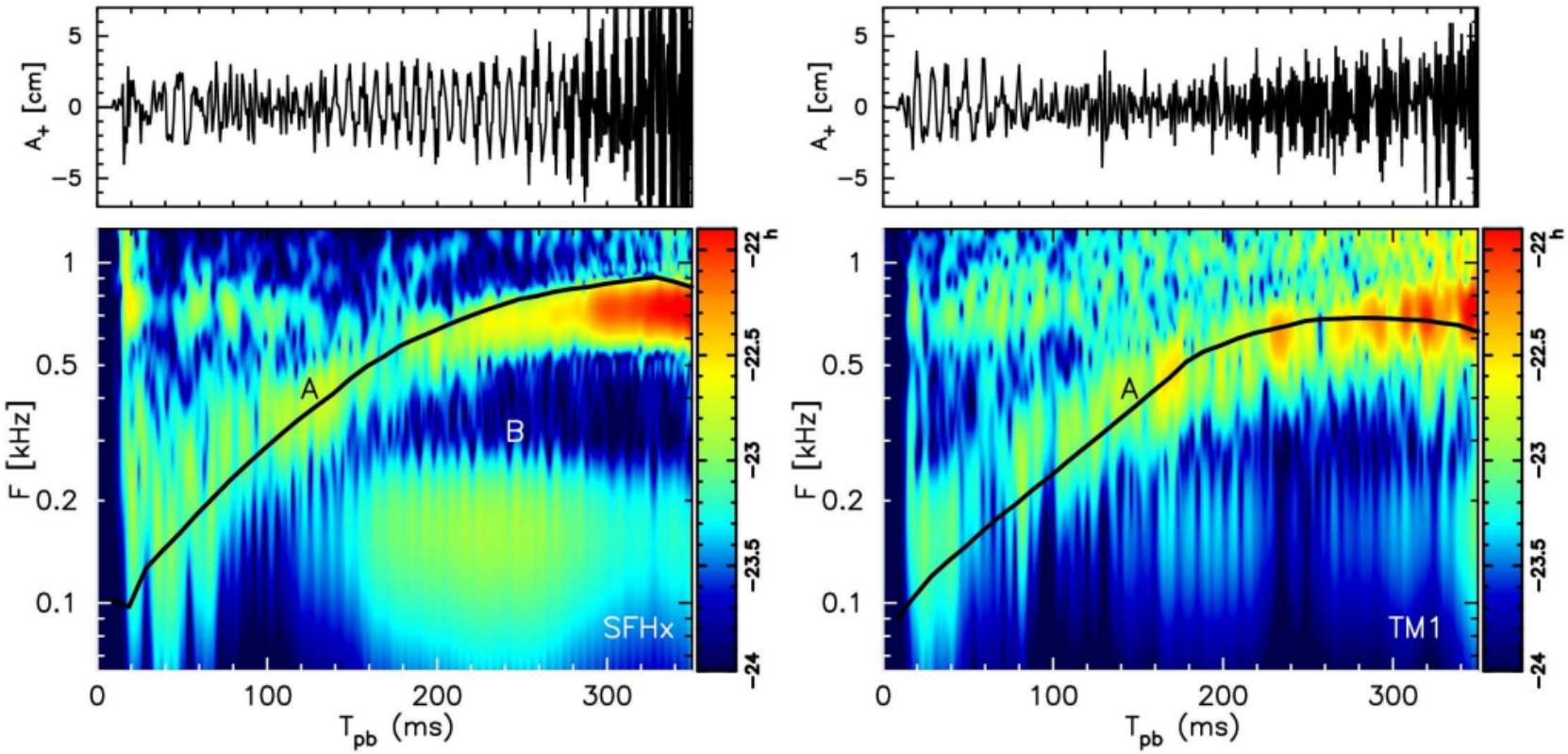

Credit: Kuroda et al. (2016)

Summary: Post-Bounce GW Signal for non-rotating models

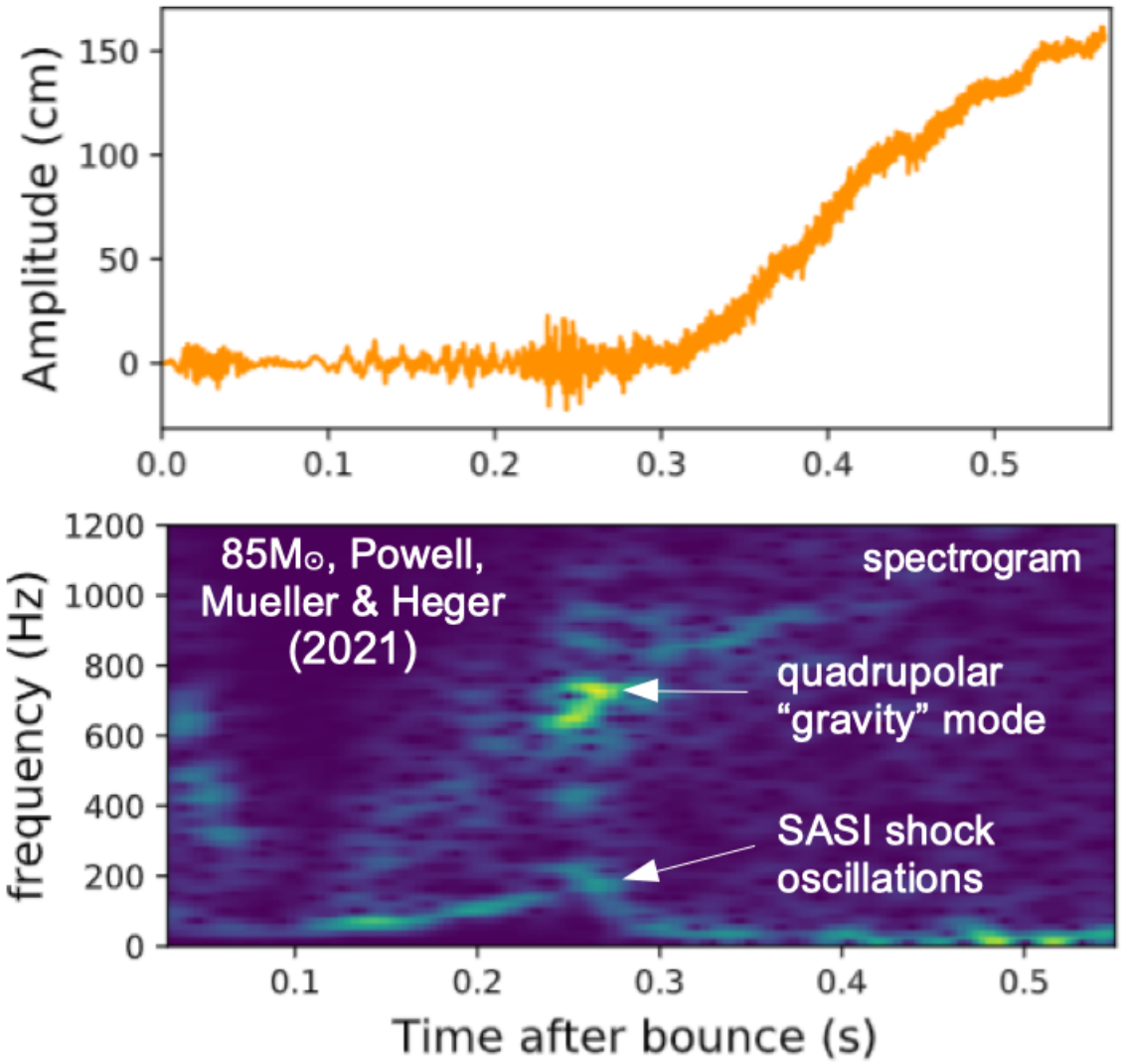

GW Signal of Rapidly Rotating Progenitors: Spiral mode

For rapidly rotating progenitors, a spiral instability (low-$|T|/|W|$ instability, distinct from the SASI spiral mode) can occur and produce a powerful GW signal.

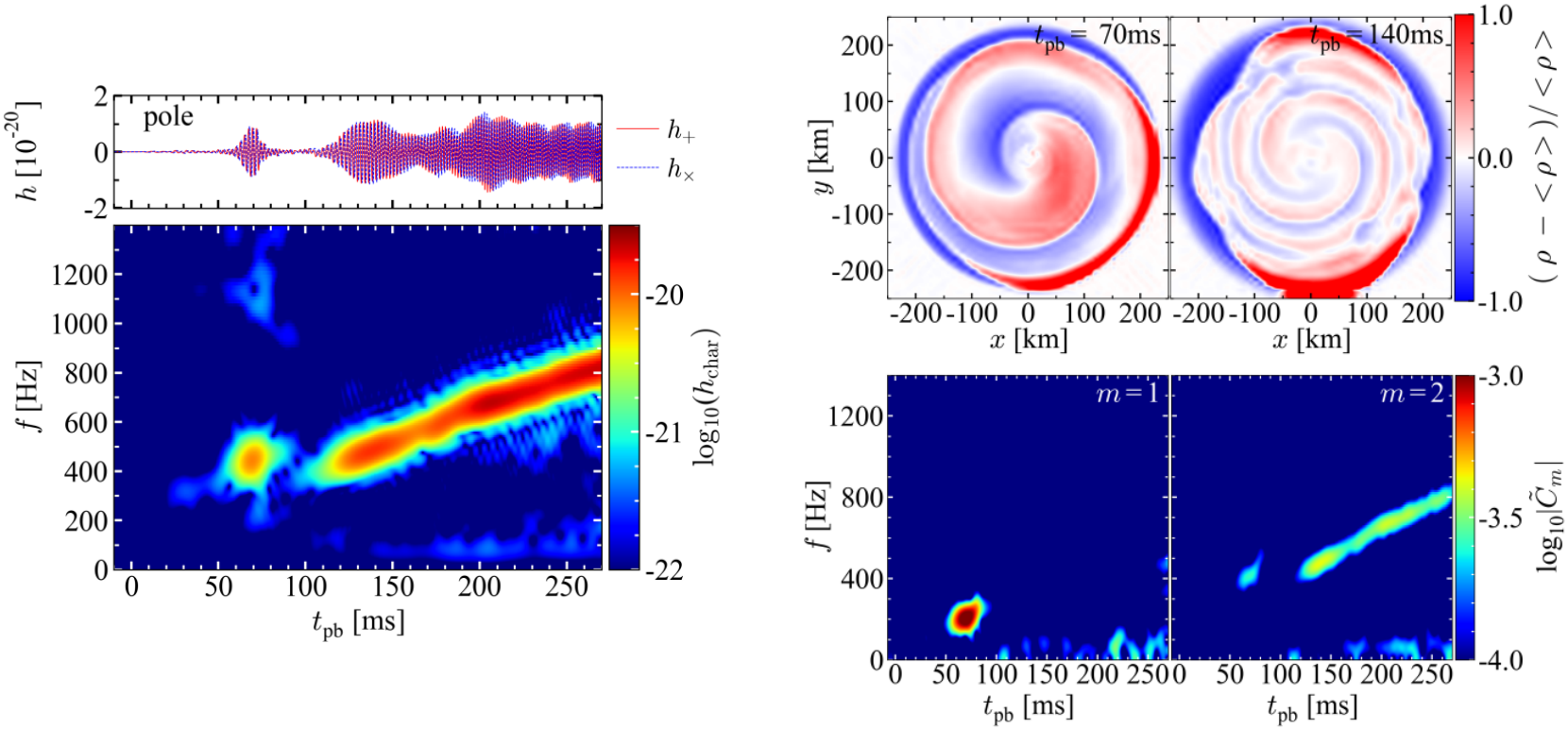

Credit: Shibagaki et al. 2020, MNRAS Letters, 493, L138
For GWs from triaxial instabilities, see also Kuroda et al. (2014), Scheidegger et al. (2010).

Detectability

The expected detectability range varies by an order of magnitude depending on progenitor mass and rotation, on explosion energy, and the presence/absence of the different signal components. Except for the SASI signal, most of the power is emitted above the optimal sensitivity range for LIGO/VIRGO/KAGRA and their planned successors.

	m39 pole	m39 eqt	s18np pole	s18np eqt	y20 pole	y20 eqt
LIGO	190 kpc	119 kpc	14 kpc	22 kpc	32 kpc	32 kpc
Virgo	90 kpc	89 kpc	12 kpc	20 kpc	18 kpc	20 kpc
KAGRA	60 kpc	77 kpc	11 kpc	18 kpc	13 kpc	18 kpc
ET-B	1.9 Mpc	1.55 Mpc	190 kpc	320 kpc	330 kpc	370 kpc
ET-D	1.9 Mpc	1.21 Mpc	155 kpc	240 kpc	330 kpc	340 kpc

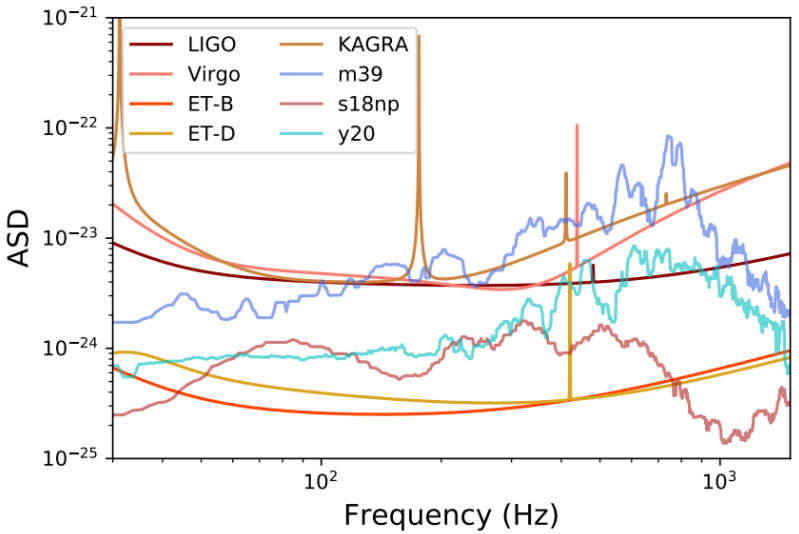

Powell & Mueller (2020)

Signal Detectability

Even close to the nominal detecability threshold of signal-to-noise ratio SNR=8, it is possible to infer signal parameters.

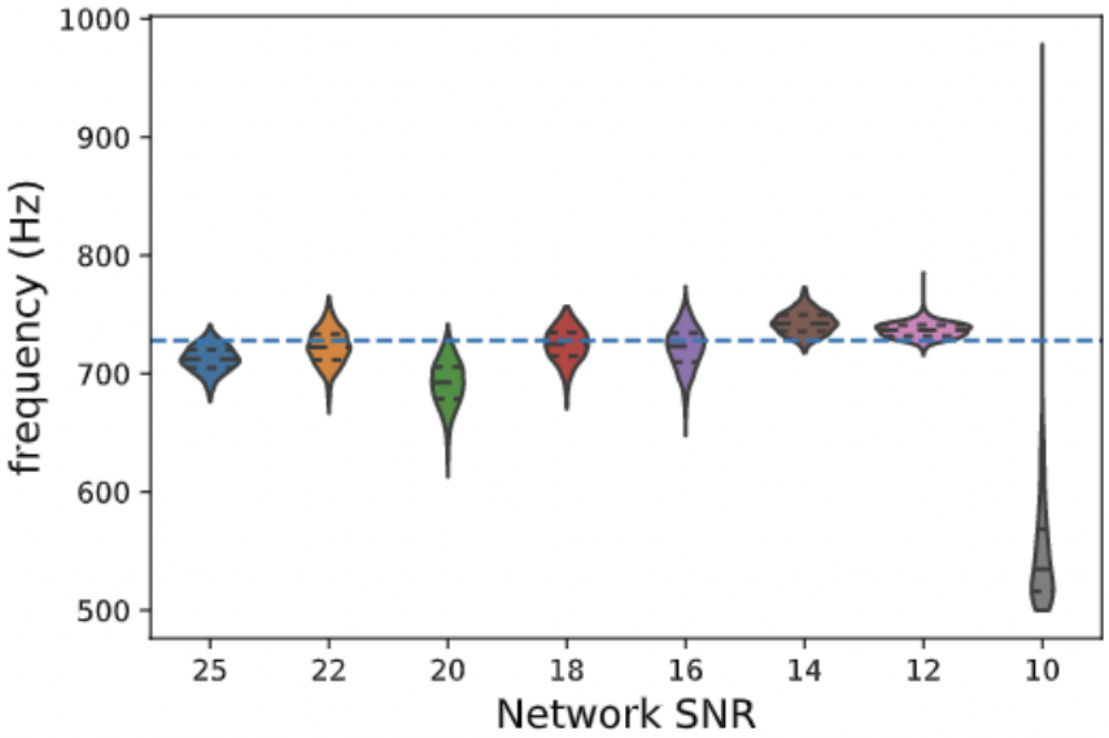

Guitar plots of posteriors as a function of SNR (Powell & Mueller 2022)

Signal Detectability

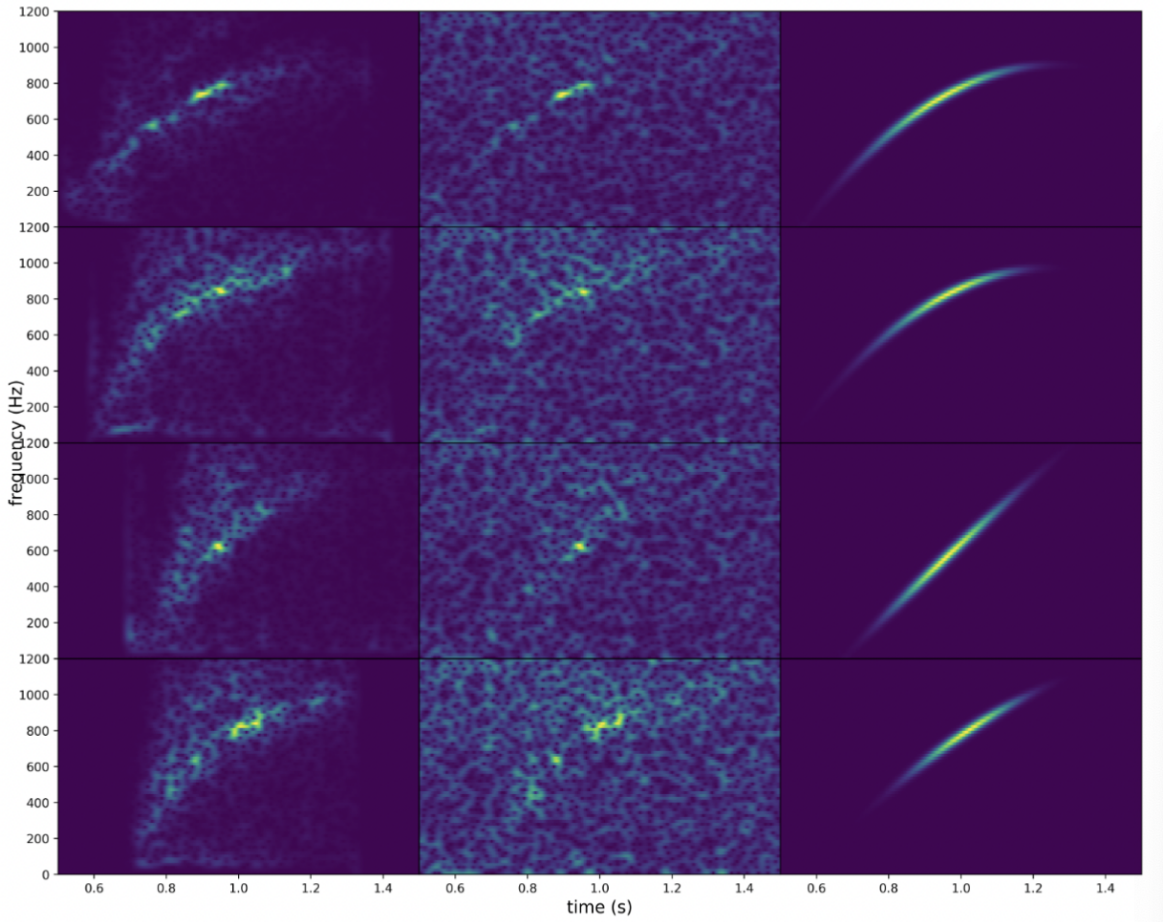

Raw, noisy, and reconstructed spectrograms for stripped and non-stripped supernova models with $39M_\odot$, $18M_\odot$, $20M_\odot$ and $3.5M_\odot$ for a fixed SNR of 25. (left to right) (Powell & Mueller 2022)

Gravitational Wave Extraction: Technical Considerations

Although relativistic effects are sizeable in the supernova core $GM/Rc^2 > 0.1$, many simulations approximate relativistic gravity by using a modified gravitational potential (Marek et al. 2008). GWs therefore need to be extracted using the quadrupole formula. Even in relativistic simulations, direct extraction from a dynamically evolved spacetime is not viable because the wave perturbations are too weak. To reduce numerical noise, the standard quadrupole formula,

$$h^{ij} = \frac{2G}{c^4 D} \frac{\partial^2}{\partial t^2} \int \rho(x^i x^j - \delta^{ij} r^2)\, \mathrm{d}^3 x,$$

is usually recast to eliminate at least one time derivative (e.g., Blanchet, Damour, & Schäfer 1990), and modified to include relativistic corrections (Mueller et al. 2013). h^{ij} then has to be projected onto the transverse trace-free part for a given observer direction.

In simulations, one sometimes runs into numerical accuracy problems when evaluating the volume integral, especially for coarse grid resolution. Note that for perfect spherical symmetry, h^{ij} should be diagonal, and the transverse trace-free part is zero for any observer. If the numerical integration does not reproduce this, one gets spurious GW ampltiudes.

Spectra and spectrograms

There are some pitfalls in the analysis of supernova waveforms, especially since spectral properties change considerably with time and since the simulations usually end before emission stops. The Fourier transform $\tilde{h}^{ij}$,

$$\tilde{h}^{ij}(f) = \int_{-\infty}^{\infty} h^{ij}(t')w(t')e^{-2\pi i f t'}\,\mathrm{d}t,$$

is the basis for computing the amplitude or power spectral density (ASD and PSD) and getting a rough estimate of the signal-to-noise ratio. The window function w for the Fourier transform of a finite-duration signal may just be a rectangular function (effectively no window) or one with tapering at the edges to optimise spectral leakage. The presence of a tail can considerably contaminate the spectrum, producing an unphysical low-frequency tail, which may be resolved by windowing. However, windowing can remove significant power from the spectrum if emission is strong at the end, and accidentally suppress signal components (e.g., the prompt convection signal. Depending on the purpose of the computed spectrum.

Spectra and spectrograms

Spectograms can be obtained using a short-time Fourier transform,

$$\tilde{h}^{ij}(t,f) = \int_{-\infty}^{\infty} h^{ij}(t')w(t'-t)e^{-2\pi ift'}\,\mathrm{d}t',$$

or, as a function of time and period p, using a Wavelet transform,

$$\hat{h}^{ij}(t,p) = \frac{1}{\sqrt{p}} \int_{-\infty}^{\infty} h^{ij}(t')\psi\left(\frac{t'-t}{p}\right)\,\mathrm{d}t',$$

where ψ is the mother wavelet (Morlet should be the default choice). The PNS and SASI oscillations are usually coherent over just a few oscillations, so the best choice is usually to use a wavelet transform with a small number of cycles. Interpreting the underlying structures of simulation data sometimes requires fine tuning, though. Beware of edge effects in spectrograms, especially for low-frequency emission from the SASI.

Neutrino Signal: Overview of Signal Phases

We can roughly distinguish three phases of the neutrino signal:

Neutronisation burst: Big spike in electron neutrino emission around bounce

Accretion phase: ν_e and $\bar{\nu}_e$ emitted with similar luminosity, somewhat higher than for ν_μ and ν_τ (from early-post bounce phase through early explosion phase)

Kelvin-Helmholtz cooling phase: All neutrino species emitted with similar luminosity but different spectra) after accretion has stopped. Transitions to volume-cooling phase after a few second when the entire neutron star becomes transparent to neutrinos (and the luminosity and mean energy is too low to observe the signal directly anymore).

Supernova Neutrino Detection

- Classical **water Cherenkov detectors** like SuperK and HyperK (planned) are primarily sensitive to $\bar{\nu}_e + p \rightarrow n + e^-$ (inverse beta decay, IBD), allow large detector volumes, and are capable of measuring the energies of detected MeV neutrinos. About 10,000 events expected in SuperK for Galactic supernova, 250,000 in HyperK. Also some events from $\nu_{\mu/\tau}$, mostly through electron scattering.
- **Long-string water Cherenkov detectors** (IceCube) achieve the largest count rates ($10^{5\ldots6}$), but no energy measurements for MeV neutrinos.
- **Liquid argon detectors** use the reaction $\nu_e + {}^{40}\mathrm{Ar} \rightarrow {}^{40}\mathrm{K} + e^-$. DUNE will sample the ν_e light curve from a Galactic supernova with $\sim 3,000$ events.
- **Liquid scintillator detectors** primarily detect $\bar{\nu}_e$ through IBD, with expected count rates of 15,000 and 5, 000 IBD events for the future JUNO and LENA detectors. Excellent energy resolution, can reconstruct ν_e signal to some extent.

Neutrino Detection

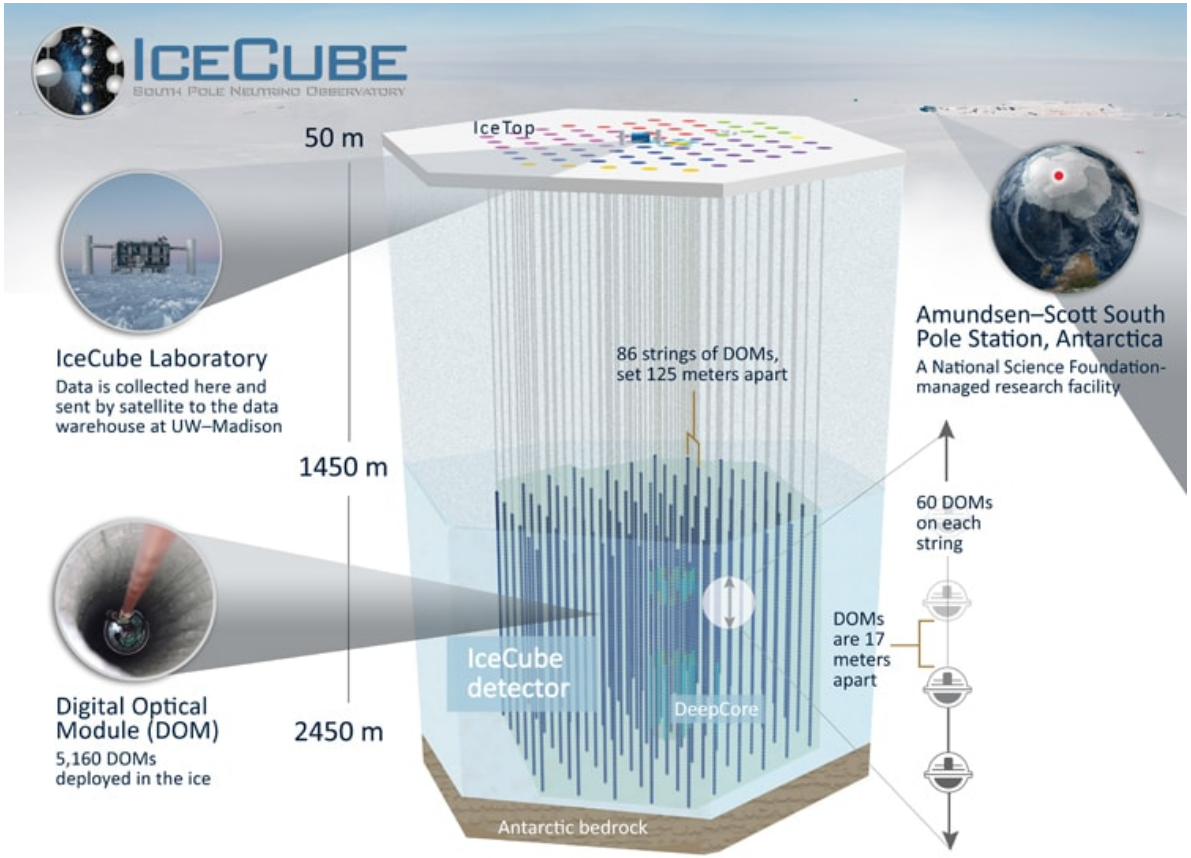

Credit: IceCube Science Team (F. Halzen, U Wisconsin), `https://icecube.wisc.edu/science/icecube/`

Problem: Flavour Conversion

The detected neutrino signal on Earth will not directly reflect the signal at the source (i.e., in the supernova core because of flvour conversion:

- Flavour conversion will inevitably occur as neutrinos leave the star due to the **MSW (Mikheyev–Smirnov–Wolfenstein) effect**. The results will depend on neutrino mixing angles and mass differences, and the mass hierarchy.
- Flavour conversion may occur deep in the supernova core due to neutrino-neutrino self-refraction. The conditions for these "collective oscillations" and their outcomes are not yet fully understood.

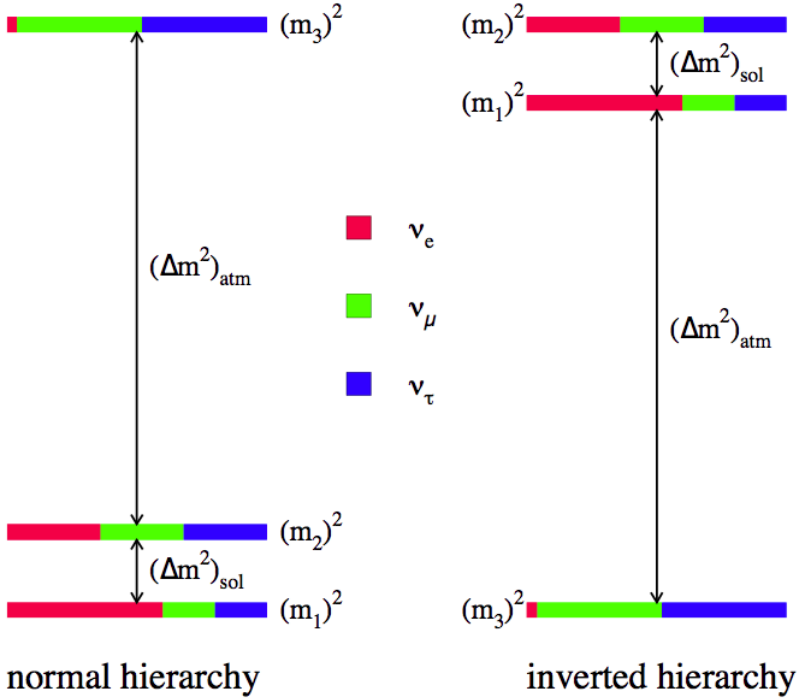

Cahn et al. (2013), arXiv:1307.5487

MSW Flavour Conversion in Supernovae

- Forward scattering on electron produces an extra potential term $\sqrt{2}G_\mathrm{F}$ for electron flavour neutrinos.
- This affects the mass eigenstates and mixing angles. For high electron density, electron and heavy-flavour neutrinos live do not mix and are aligned with mass eigenstates.
- When the neutrinos move out through a region with $\sqrt{2}G_\mathrm{F} \sim \Delta m_{12} c^2$ (at $\sim 10\,\mathrm{g\,cm^{-3}}$, L-resonance) or $\sqrt{2}G_\mathrm{F} \sim \Delta m_{23} c^2$ (at $\sim 10^3\,\mathrm{g\,cm^{-3}}$, H-resonance) , flavour conversion will occur.
- If n_e changes slowly over an oscillation length (adiabatic conversion), the neutrinos stay in the same mass eigenstate (with different flavour structure), otherwise they go into an oscillating superposition of vacuum mass eigenstates.
- Rule of thumb:
  - Normal hierarchy: ν_e completely swap with heavy-flavour neutrinos, $\bar{\nu}_e$ have survival probability ~ 0.68.
  - Inverted hierarchy: ν_e have survival probability ~ 0.32, $\bar{\nu}_e$ have survival probability 0.
  - Further complications: Turbulence in resonance region, sterile neutrinos.

Collective Oscillations

- In a dense neutrino gas, the effective Hamiltonian for a neutrino travelling with velocity $\mathbf{v}$ is $H = H_{\rm vac} + \sqrt{2} G_{\rm F} \left(n_e + \int (\rho' - \bar{\rho}')(1 - \mathbf{v}' \cdot \mathbf{v}) \, {\rm d}^3 p' \right)$ in terms of the neutrino density matrix ρ, $\bar{\rho}$ for neutrinos an antineutrinos.
- If the self-refractive term is important, flavour conversion becomes a collective phenomenon.
- Instability to collective flavour conversion is associated with crossings of the neutrino distribution function for different species (f_{ν_e} with $f_{\bar{\nu}_e}$ or $f_{\nu_e}, f_{\bar{\nu}_e}$ with $f_{\nu_{\mu/\tau}}$). Some instabilities are suppressed if $n_e \gg n_\nu$.
- Collective flavour conversion is probably suppressed during the burst phase, probably relevant for the neutrino-driven wind phase. Its role during the accretion and early explosion phase if most difficult o understand.

Neutrino Signal: Overview of Signal Phases

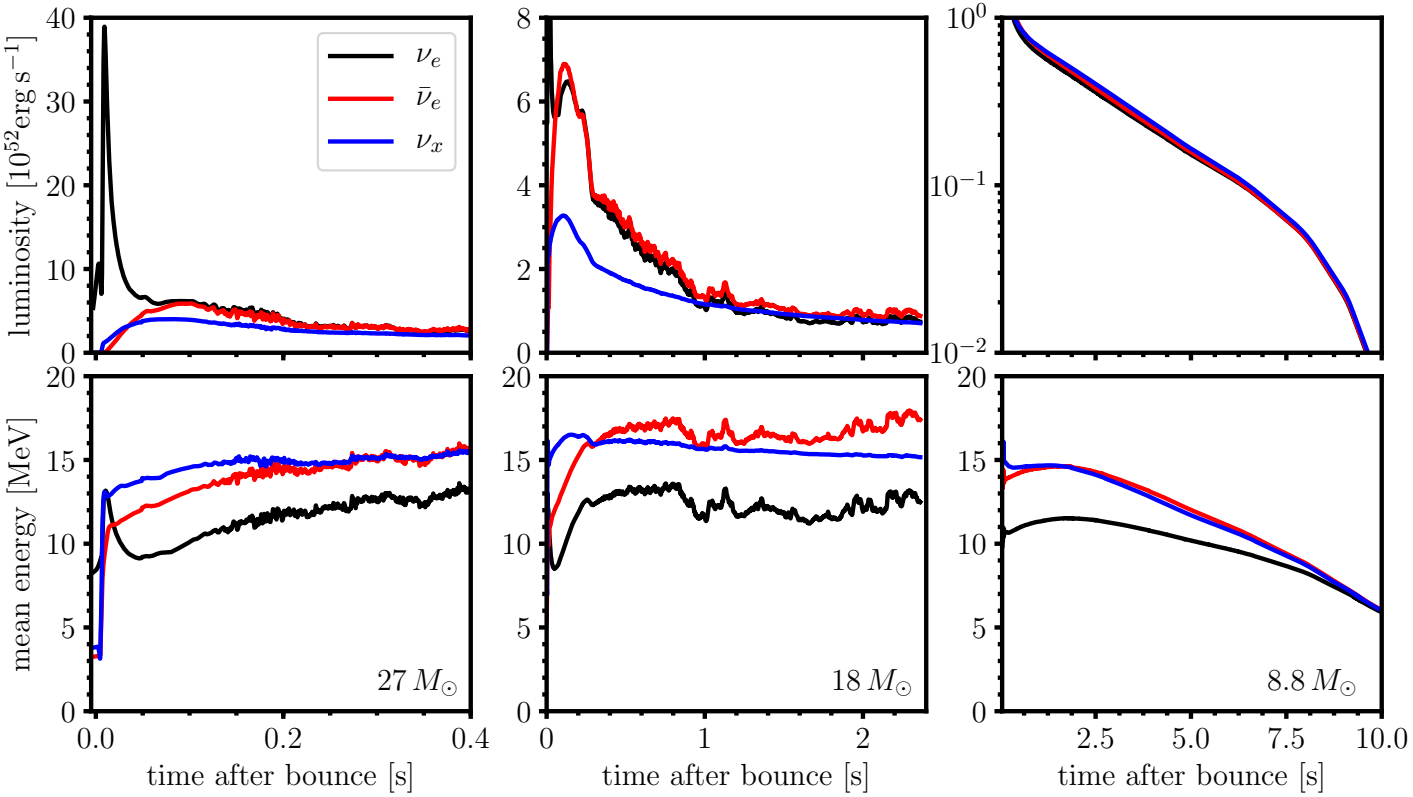

Left: burst and accretion Phase. Middle: Accretion phase and transition to cooling phase. Right: Cooling phase.

Neutronisation Burst

- ν_e-burst when shock reaches density of $\sim 10^{11}\,\mathrm{g\,cm^{-3}}$ as matter jumps from $Y_e \sim 0.5$ to hot β-equilibrium
- Burst is very **uniform** across progenitors (peak luminosity $\sim 3.5 \times 10^{53}\,\mathrm{erg\,s^{-1}}$
- Burst could pinpoint SN distance within 5% (Kachelrießet al. 2005) in megaton Water Cherenkov detctor like HyperK (electron scattering channel
- ν_e-burst and the concurrent rise in $\bar{\nu}_e$ and ν_μ/τ emission can help time the bounce to within a few ms (e.g., Halzen & Raffelt 2009) $\rightarrow$import timestamp for GW detection

Burst Signal in DUNE

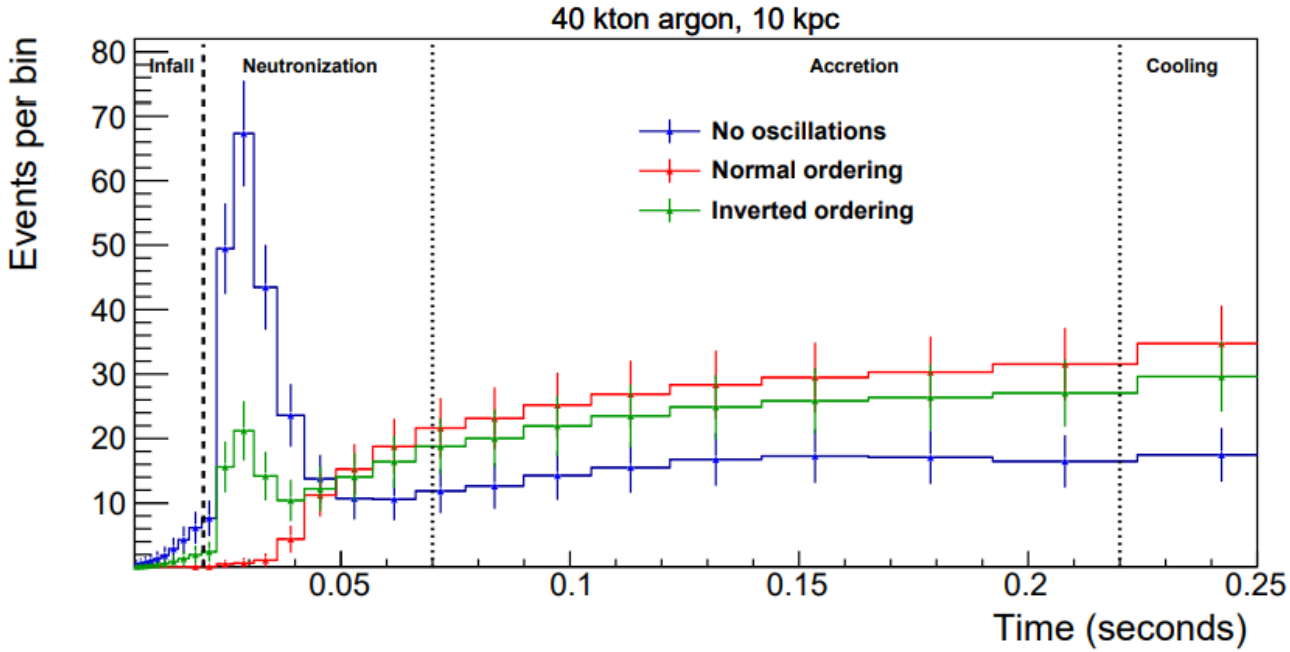

Abi et al. (DUNE Collaboration) 2020, arXiv:2008.06647

Neutrino Interaction and Equation of State Regimes during the Accretion Phase

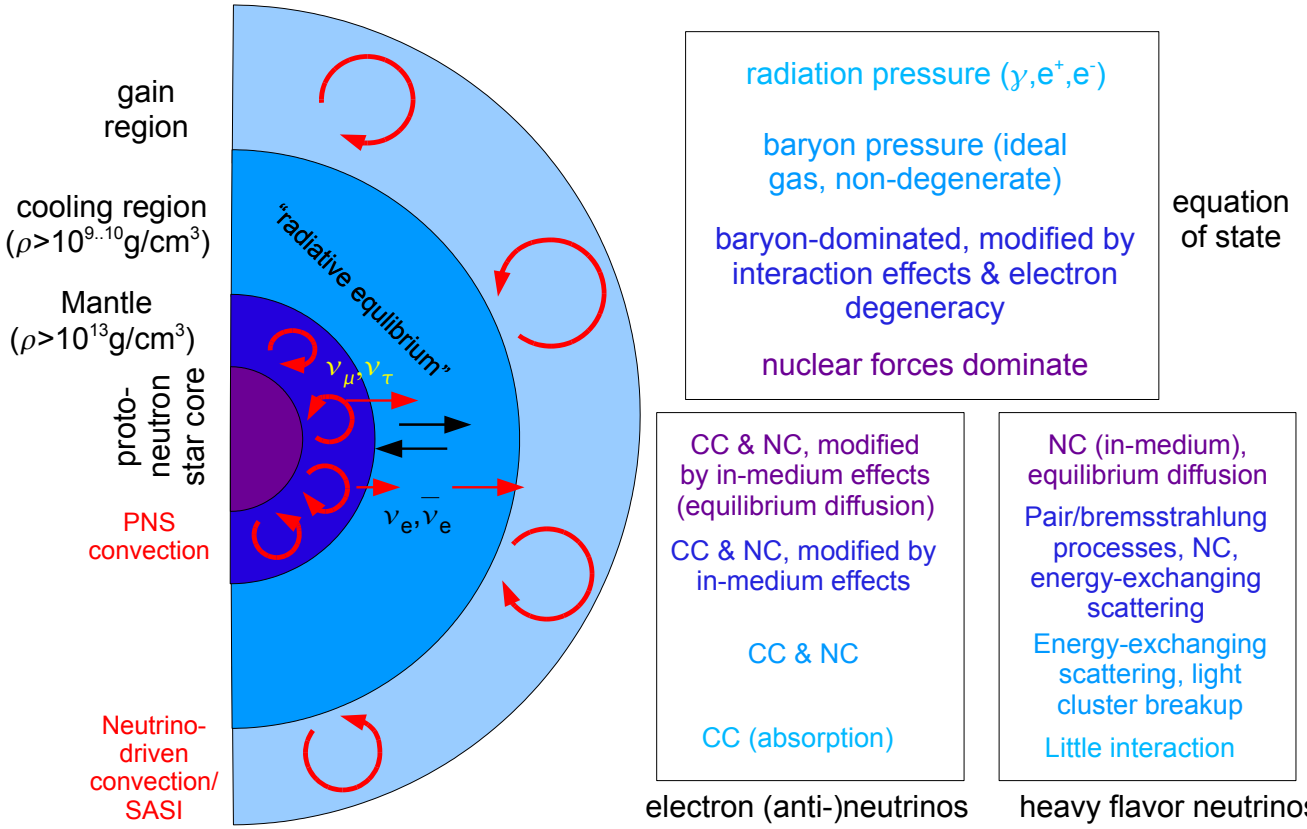

(cp. discussion during lecture on supernova dynamics)

Neutrino Luminosities and Mean Energies

- ν_e and $\bar{\nu}_e$ are mostly produced by charged current reactions (s $p + e^- \rightarrow \nu_e$ and $n + e^+ \rightarrow \bar{\nu}_e$), mostly in the cooling region from accretion power
- Diffusive flux from the mantle to the neutrinosphere for all flavours: $L_{\mathrm{diff}} \sim 4\pi\phi\sigma_{\mathrm{Fermi}} R^2 T^4$ with greyness factor $\phi \approx 0.4 \ldots 0.6$
- Fit from Mirizzi et al. (2016): $L_{\nu_e} + L_{\bar{\nu}_e} \frac{GM\dot{M}}{R_{\mathrm{PNS}}}$ with $\beta_1 = 1.25$ $\beta_2 = 0.5$
- The luminosities for ν_e and $\bar{\nu}_e$ tend to be similar. The ν_e *number* flux is higher, however, since the accreted material needs to lose lepton number to get into β-equilibrium at the proto-neutron star surface.
- The neutrino mean energies reflect the temperature at the neutron star surface, which is related to its bulk parameters as well. The mean energy of $\bar{\nu}_e$ is roughly $\langle E_{\bar{\nu}_e} \approx 10\,\mathrm{MeV}(M/M_\odot)$. However, the details are more complicated.

Spectrum Formation – ν_e and $\bar{\nu}_e$

Neglecting final state blocking and other many-body effects for nucleons and electrons/positrons, the charged current cross sections for ν_e and $\bar{\nu}_e$ scale as

$$\sigma_{\nu_e+n\to p+e^-} \propto n_n(\epsilon+q)\sqrt{(\epsilon+q)^2-m_e^2c^4},$$
$$\sigma_{\bar{\nu}_e+p\to n+e^+} \propto n_p(\epsilon-q)\sqrt{(\epsilon-q)^2-m_e^2c^4},$$

where $q = m_n - m_p = 1.29\,\mathrm{MeV}$.
This has two important consequences:

- The ν_e opacity is generally higher because $n_n > n_p$, and because of the proton-neutron mass difference term. Hence they decouple slightly further out at lower temperature and have smaller mean energy.
- Since the opacity increases with neutrino energy, the neutrinosphere radius is located further out at lower temperatures for high-energy neutrinos. Since the emerging flux is determined by the equilibrium distribution function $f = 1/(1+\exp(E-\mu)/tT)$ at the neutrinosphere. The spectrum of ν_e and $\bar{\nu}_e$ is therefore "pinched" at high energy compared to a Fermi-Dirac spectrum.

Spectrum Formation – Heavy Flavour Neutrinos

The number flux of ν_μ and ν_τ is determined at high densities where they can be produced by various pair processes. However, they are still trapped at lower densities by the high neutrino-nucleon scattering opacity, and can exchange energy with the medium by scattering on nucleons and electrons. Downscattering brings the average energy of $\nu_{\mu/\tau}$ below that of $\bar{\nu}e$ a few hundred milliseconds after collapse. However, their spectral *shape* still less pinched.

Spectrum Formation – Heavy Flavour Neutrinos

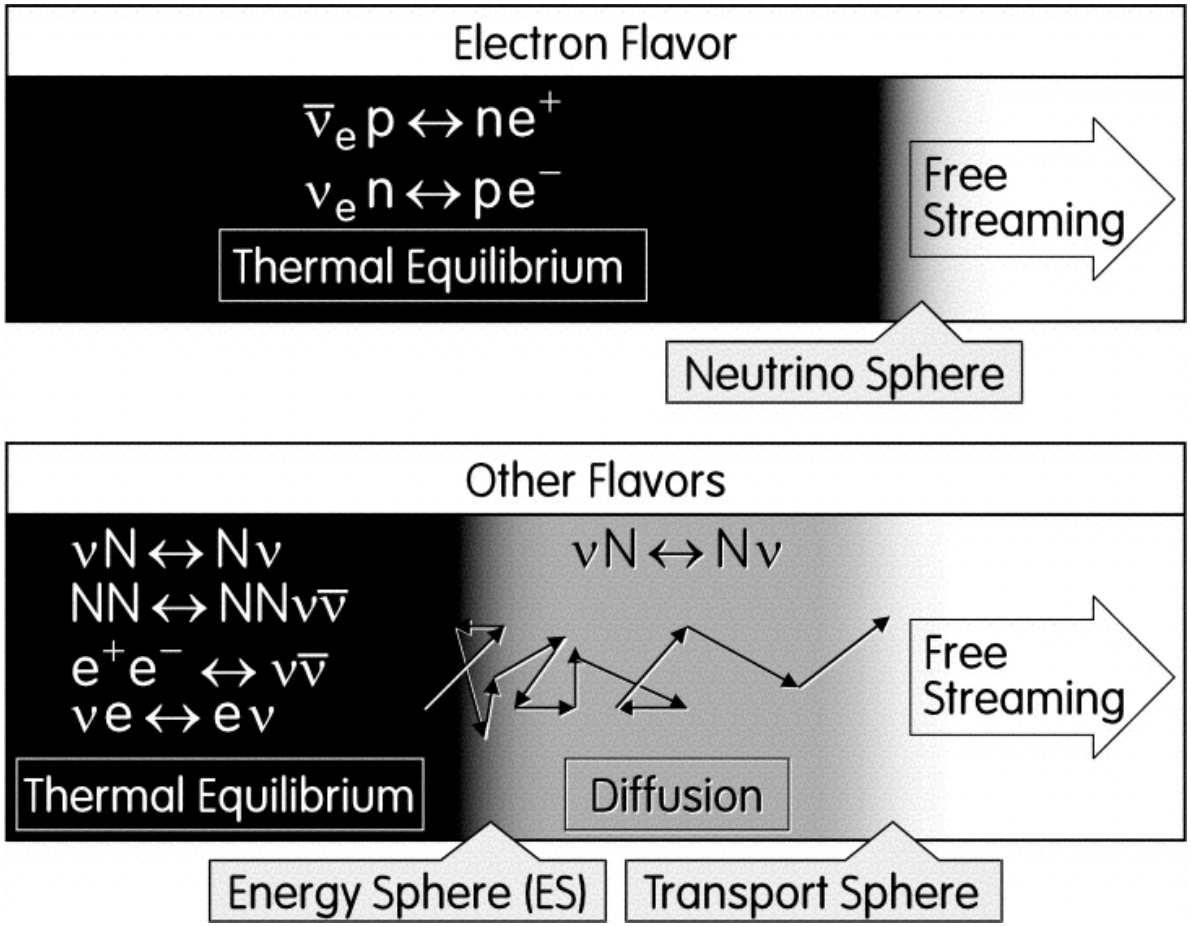

Credit: Raffelt (2001)

Implications of Non-Thermal Spectra

The pinching of the spectral tail is important for the neutrino detection event rate as the IBD cross section also scales with ϵ^2, and some detection channels (charged current on Pb, neutral current on O) have high effective threshold values.
As a convenient spectral fit, one can use a generalised Boltzmann distribution in terms of the mean neutrino energy $\langle E \rangle$ with a shape parameter α

$$F \propto E^{\alpha} e^{-(\alpha+1)E/\langle E \rangle}.$$

During the accretion phase, $\alpha \sim 2.65$ for ν_e, $\alpha \sim 3.1$ for $\bar{\nu}_e$, and $\alpha \sim 2.4$ for $\nu_{\mu\tau}$ provides a good approximation. for ν_e become more strongly pinched (higher α) with time, and $\bar{\nu}_e$ become less pinched (Tamborra et al. 2013).

Inferring Progenitor and Proto-Neutron Star Properties

In principle, one could use the flavour-dependent neutrino fluxes and mean energies to constrain the neutron star mass M, radius R, and accretion rate $\dot{M}$. The temporal history of $\dot{M}$ can be related directly to the progenitor structure. However, uncertainties about flavour conversion and limited flavour-dependent information make it harder to extract quantitative time-dependent information on physical parameters. Quantitative statements about global proto-neutron star or progenitor parameters will be more readily forthcoming:

- Even for massive progenitor with high accretion luminosity, the total radiated energy is almost shared equally between flavours (to about 20%. This allows an estimate of the neutron star binding energy ($E_{\mathrm{bind}} \sim M^2$).
- O'Connor & Ott (2013): Time-integrated electron antineutrino flux over the first $0.5\,\mathrm{s}$ can constrain the progenitor compactness despite uncertainties about EoS and flavour conversion.
- About two dozen neutrinos from SN 1987A provided some quantitative information: compact object with a binding energy of a few $10^{53}\,\mathrm{erg}$, signal duration of a few second, neutrinosphere radius of tens of km, temperature of a few MeV.

Progenitor Dependence of Neutrino Emission

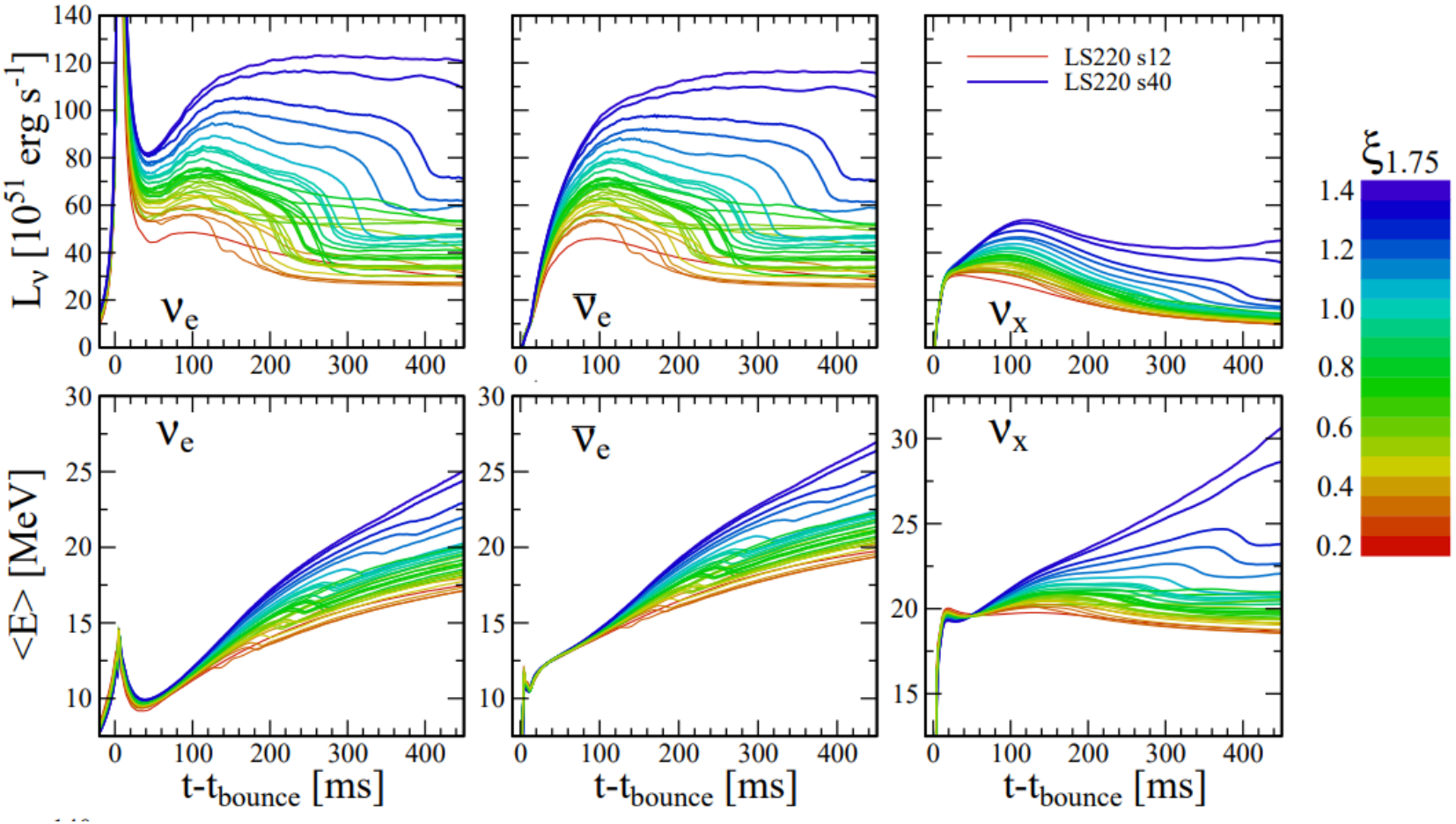

O'Connor & Ott (2013):

Progenitor Dependence of Neutrino Emission

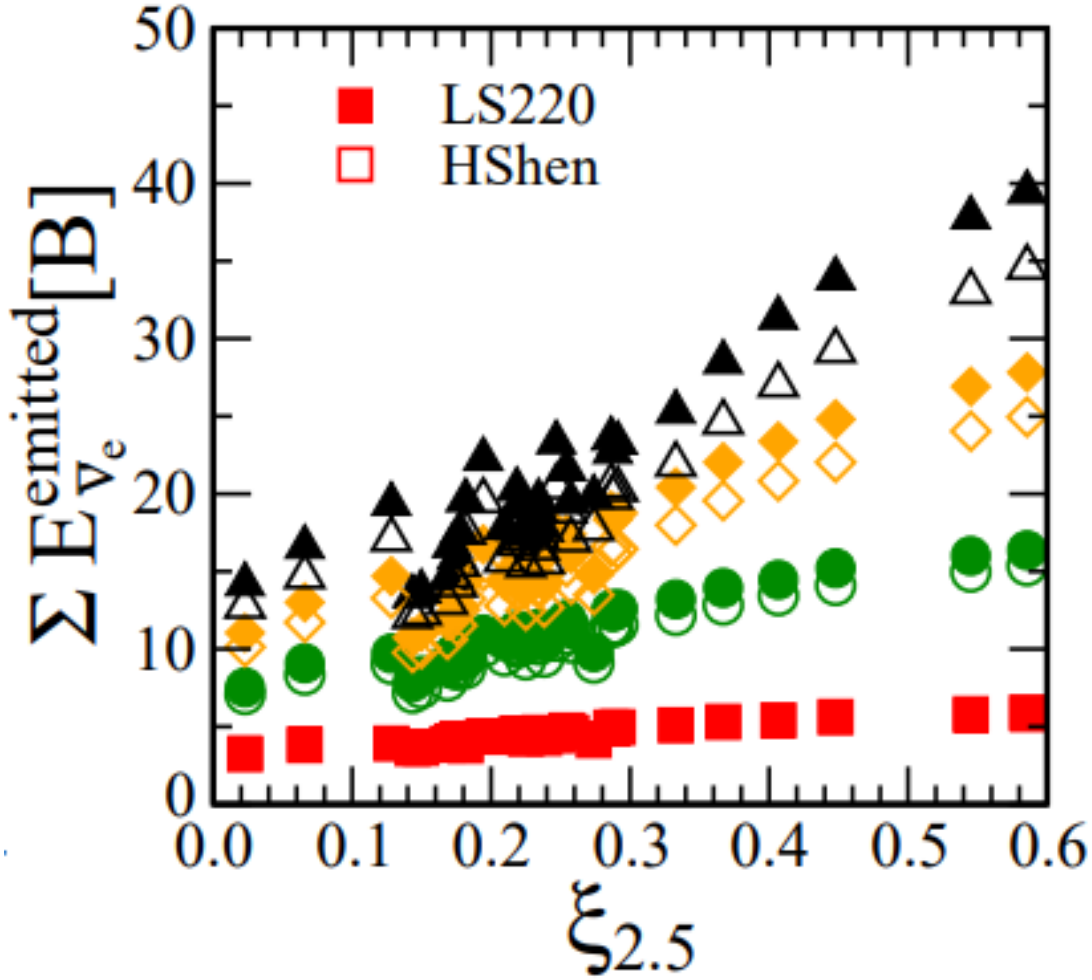

O'Connor & Ott (2013):

Neutrinos as a Probe of Multi-Dimensional Dynamics

- The standing-accretion shock instability (SASI) results in a strongly asymmetric and variable accretion flow onto the proto-neutron star. This translates into an observable oscillations in the ν_e- and $\bar{\nu}_e$-flux for suitable observer directions.
- The modulation period is related to the shock and PNS radius, $T_{\mathrm{SASI}} = 19\,\mathrm{ms}\left(\frac{r_{\mathrm{sh}}}{100\,\mathrm{km}}\right)^{3/2} \ln\left(\frac{r_{\mathrm{sh}}}{R}\right)$. Its time dependence can be measured with a short-time Fourier or Wavelet transform of IceCube od HyperK count rates.
- Modulation periods longer than $20\,\mathrm{ms}$ likely indicate explosion.
- If fallback occurs during early explosion phase, this will leave characteristic mini-bursts in the neutrino signal.

SASI Signal

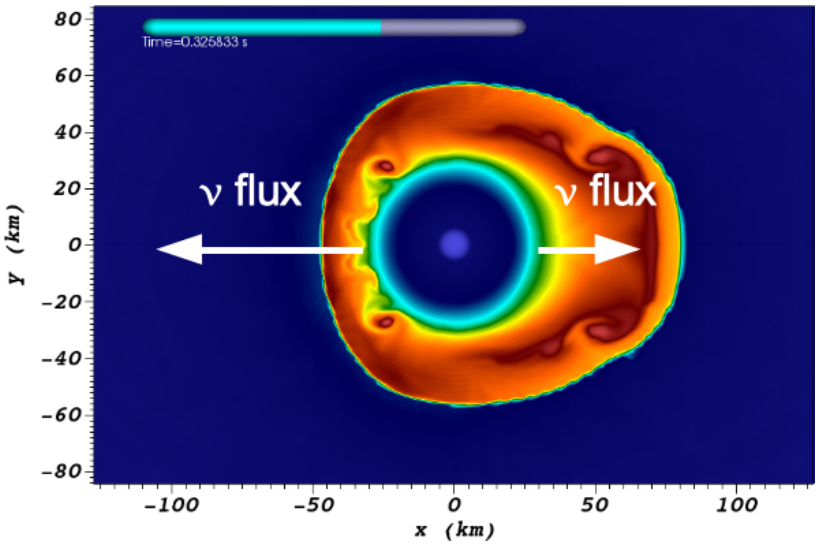
Time=0.325833 s
ν flux
ν flux
y (km)
x (km)
80
60
40
20
0
-20
-40
-60
-80
-100
-50
0
50
100

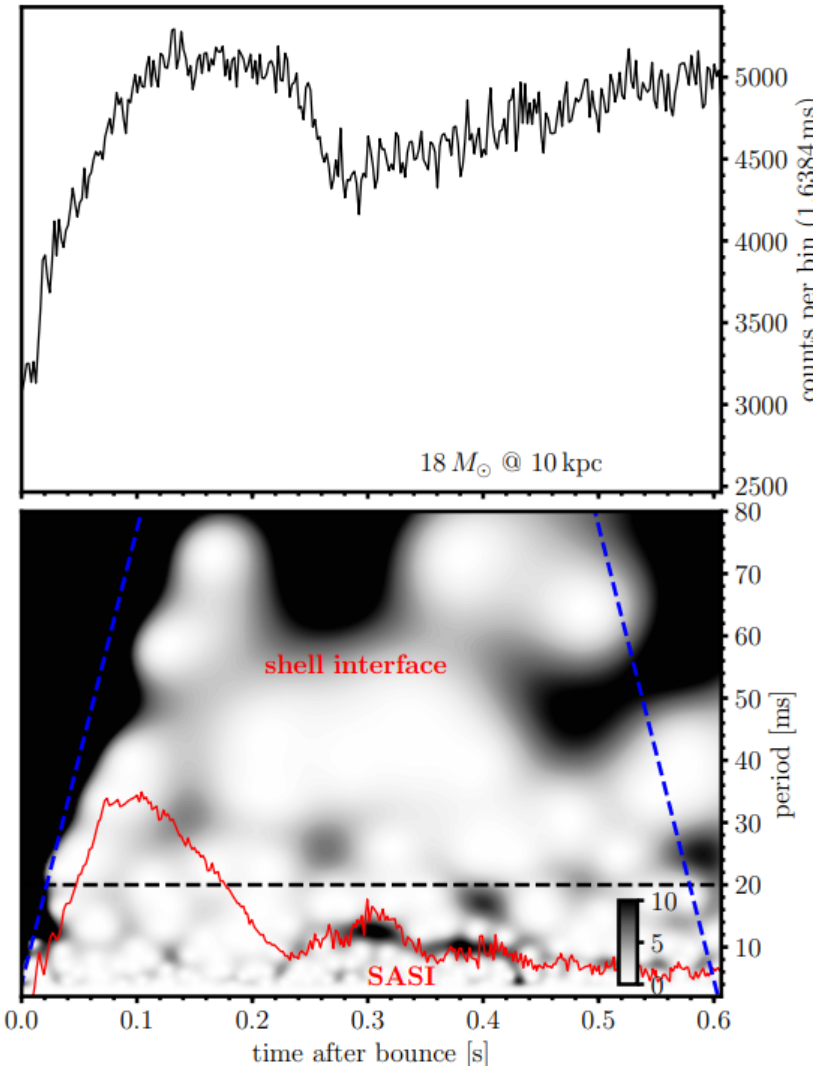
18 $M_\odot$ @ 10 kpc
counts per bin (1.6384 ms)
5000
4500
4000
3500
3000
2500
shell interface
SASI
period [ms]
80
70
60
50
40
30
20
10
10
5
0
0.0
0.1
0.2
0.3
0.4
0.5
0.6
time after bounce [s]

Fallback Signal

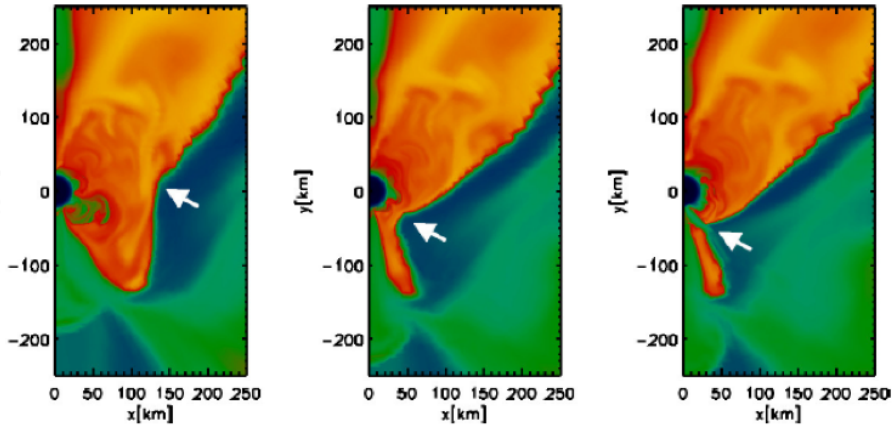

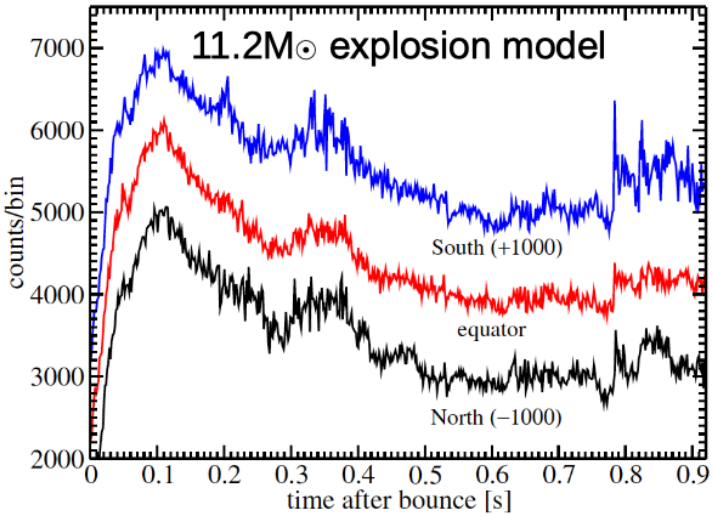

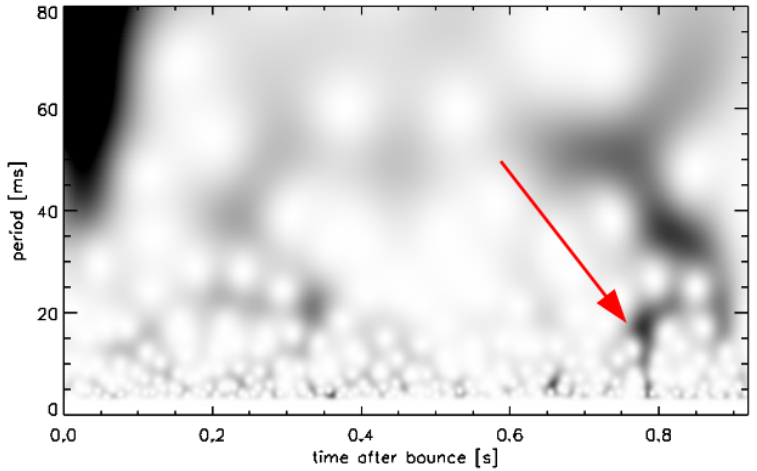

Phase Transition Signature

Secondary neutrino bursts might also result from a phase transition in the proto-neutron star. A strong first-order phase transition to quark matter can lead to a second collapse and bounce, and launch an electron *anti*neutrino burst (Sagert et al. 2009, Dasgupta et al. 2010).

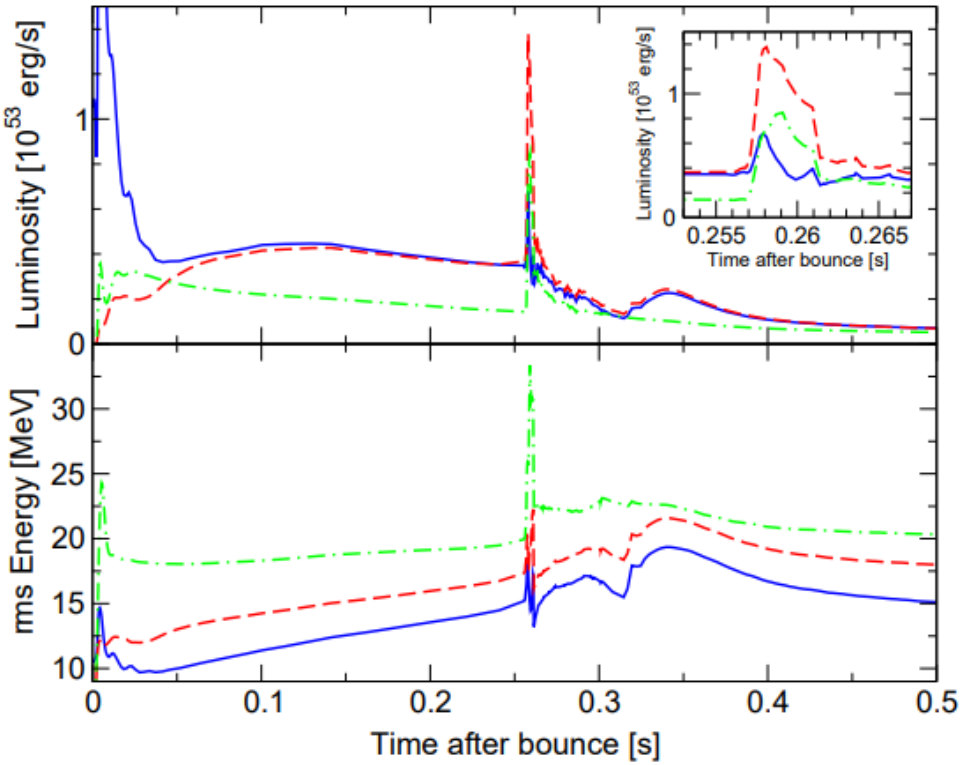

Credit: Dasgupta et al. (2010)

Further Potential of Supernova Neutrino Detection

- Constraining high-density equation-of-state physics (e.g., symmetry energy) using the signal from the Kelvin-Helmholtz cooling phase
- Constraints neutrino physics parameters (mass hierarchy) or exotic physics (e.g., axions)
- Effect of hydrodynamic turbulence in the MSW resonance regions on flavour conversion
- ...